The Astrophysical Journal Letters, 877:L7 (6pp), 2019 May 20 https://doi.org/10.3847/2041-8213/ab1fdd

The Galactic Disk Phase Spirals at Different Galactic Positions Revealed by *Gaia* and LAMOST Data

C. Wang[1,8], Y. Huang[2], H.-B. Yuan[3], M.-S. Xiang[4,5], B.-Q. Chen[2], H.-F. Wang[2,6,8], Y.-Q. Wu[5], H.-W. Zhang[1], Z.-J. Tian[7], Y. Yang[2], M. Zhang[1], and X.-W. Liu[2]

[1] Department of Astronomy, Peking University, Beijing 100871, People's Republic of China; wchun@pku.edu.cn
[2] South-Western Institute for Astronomy Research, Yunnan University, Kunming, Yunnan 650091, People's Republic of China; x.liu@ynu.edu.cn
[3] Department of Astronomy, Beijing Normal University, Beijing 100875, People's Republic of China
[4] Max-Planck Institute for Astronomy, Konigstuhl, D-69117, Heidelberg, Germany
[5] National Astronomical Observatories, Chinese Academy of Sciences, Beijing 100012, People's Republic of China
[6] Department of Astronomy, China West Normal University, Nanchong 637009, People's Republic of China
[7] Department of Astronomy, Yunnan University, Kunming 650200, People's Republic of China
Received 2019 January 30; revised 2019 March 20; accepted 2019 March 22; published 2019 May 20

Abstract

We have investigated the distributions of stellar azimuthal and radial velocity components V_Φ and V_R in the vertical position–velocity plane Z–V_Z across the Galactic disk of $6.34 \lesssim R \lesssim 12.34$ kpc and $|\Phi| \lesssim 7.^\circ5$ using a *Gaia* and *Gaia*-LAMOST sample of stars. As found in previous works, the distributions exhibit significant spiral patterns. The V_R distributions also show clear quadrupole patterns, which are the consequence of the well-known tilt of the velocity ellipsoid. The observed spiral and quadrupole patterns in the phase space plane vary strongly with radial and azimuthal positions. The phase spirals of V_Φ become more and more relaxed as R increases. The spiral patterns of V_Φ and V_R and the quadrupole patterns of V_R are strongest at $-2^\circ < \Phi < 2^\circ$ but negligible at $4^\circ < \Phi < 6^\circ$ and $-6^\circ < \Phi < -4^\circ$. Our results suggest an external origin of the phase spirals. In this scenario, the intruder, most likely the previously well-known Sagittarius dwarf galaxy, passed through the Galactic plane in the direction toward either Galactic center or anti-center. The azimuthal variations of the phase spirals also help us constrain the passage duration of the intruder. A detailed model is required to reproduce the observed radial and azimuthal variations of the phase spirals of V_Φ and V_R.

Key words: Galaxy: disk – Galaxy: kinematics and dynamics – Galaxy: structure

1. Introduction

It is recognized that the Milky Way is not steady and axisymmetric. The stellar populations of the Milky Way disk are perturbed by non-axisymmetric structures, including the Bar, the Spiral arms, the halo substructures, and the satellite dwarf galaxies (Siebert et al. 2012; Gómez et al. 2013; Bovy et al. 2015), and therefore show significant phase spirals (Antoja et al. 2018; Bland-Hawthorn et al. 2019; Tian et al. 2018), as well as radial motions and vertical bulk motions (Siebert et al. 2011; Carlin et al. 2013; Williams et al. 2013; Sun et al. 2015; Huang et al. 2016; Carrillo et al. 2018; Wang et al. 2018). Studying those phase spirals and bulk motions can help us understand the perturbation history of the Milky Way (disk).

Antoja et al. (2018) first detected the remarkable phase spirals in the local stellar disk. They found that the distributions of stellar radial and azimuthal velocity components V_R and V_Φ show significant spiral patterns in the vertical position–velocity plane Z–V_Z. Further works have studied the variations of the phase spirals with stellar age, action, chemistry, and disk position using the Large Sky Area Multi-Object Fibre Spectroscopic Telescope (LAMOST)-*Gaia* (Tian et al. 2018) and the Galactic Archaeology with HERMES (GALAH)-*Gaia* (Bland-Hawthorn et al. 2019) data. Their results not only confirm the original remarkable discovery of Antoja et al. (2018), but also resolve significant variations of the phase spirals with aforementioned parameters. Tian et al. (2018) found that the spirals are gradually apparent from $\tau < 0.5$ Gyr, and then slowly disappear until $\tau > 6.0$ Gyr. Bland-Hawthorn et al. (2019) showed that the phase spirals are more easily discerned in the distributions of α-poor stars than those of α-rich stars. They also find that the spiral is clearest in stars with smaller action J_r, and tighter in stars with smaller angular momentum L_z. The radial and azimuthal variations of phase spirals were also found by Bland-Hawthorn et al. (2019) and Laporte et al. (2019). It is worth noting that the sample of Bland-Hawthorn et al. (2019) only covers a small distance range of 1 kpc from the Sun and Laporte et al. (2019) does not study the azimuthal variations of phase spirals; the spatial variations of the phase spirals need to be explored in a larger volume of the Galactic disk.

In the theoretical view, several works have attempted to explain the observed phase space spiral patterns by either external (Antoja et al. 2018; Binney & Schönrich 2018; Bland-Hawthorn et al. 2019; Laporte et al. 2019) or internal (Khoperskov et al. 2018) perturbations. Both scenarios can reproduce the phase spirals of V_Φ and V_R in the Solar neighborhood. Antoja et al. (2018), Binney & Schönrich (2018), Bland-Hawthorn et al. (2019), and Laporte et al. (2019) suggested that the phase spirals are probably the consequence of the Sagittarius dwarf galaxy perturbation. Independent to the external perturbation scenario, Khoperskov et al. (2018) suggested that the observed phase space spirals can be produced naturally by vertical oscillations driven by the buckling of the stellar bar—there is no need for an external perturber (a massive satellite or a sub-halo), whereas simulations considering external or internal perturbations predict different spatial variations of the phase spirals. In the external

[8] LAMOST Fellow.

scenario, Bland-Hawthorn et al. (2019) implied tighter phase space spirals in the inner disk due to faster vertical oscillations leaded by a stronger disk gravity in the inner disk. Khoperskov et al. (2018) have also predicted the properties of phase space spirals in different R and Φ bins considering internal perturbations, but did not find a tighter phase space spirals in the inner disk. Thus, studying the phase space spirals at different disk positions in a larger volume of the disk can no doubt distinguish the origins of the phase spirals. Unfortunately, the radial and azimuthal variations of the phase spirals are not well studied yet.

In the current work, we study the phase space spirals at different disk positions (R and Φ), in particular its radial variations, to see whether the phase space spirals in the inner disk are tighter as predicted by the scenario of Bland-Hawthorn et al. (2019). Our work is based on the recently released *Gaia* second data release (DR2), which provides precise proper motions and distances for more than 1.3 billion stars, and precise line-of-sight velocities for more than 7 million stars. In addition, the LAMOST surveys have yielded precise line-of-sight velocities and metallicities for millions of stars. These data enable us to derive accurate 3D velocities for large samples of stars across the Galactic disk ranging from 6 to 12 kpc, thus allowing us to examine the spatial variations of the phase space spirals across a wide range of the disk.

This Letter is organized as follows. In Section 2, we briefly introduce the samples used. In Section 3, we present the main results. The discussions are presented in Section 4. Finally, we summary our work in Section 5.

2. Data

2.1. Coordinate Systems

We use the Galactocentric cylindrical system (R, Φ, Z) with R, the projected Galactocentric distance, increasing radially outward, Φ in the direction of the Galactic rotation, and Z toward the North Galactic Pole. The Sun is assumed to be at the Galactic midplane (i.e., $Z_0 = 0$ pc) and has a value of R_0 of 8.34 kpc (Reid et al. 2014). We adopt a local circular speed of rotation curve of $V_c(R_0) = 240\ \mathrm{km\ s^{-1}}$, and solar motions $(U_\odot, V_\odot, W_\odot) = (11.1,\ 12.24,\ 7.25)\ \mathrm{km\ s^{-1}}$ relative to the local standard of rest (Schönrich et al. 2010). The results presented in the current work are stable if we choose $Z_0 = 27$ pc and other solar motions relative to the local standard of rest (Huang et al. 2015).

2.2. The Stellar Samples

By 2016 June, ~6.5 million stellar spectra of signal-to-noise ratios higher than 10 for 4.4 million unique stars have been obtained with LAMOST (Xiang et al. 2017a) during the Pilot Surveys and the first four years of the five-year Phase I Regular Surveys of the LAMOST Galactic spectroscopic surveys (Deng et al. 2012; Zhao et al. 2012; Liu et al. 2014; Yuan et al. 2015). Stellar atmospheric parameters (effective temperature $T_{\rm eff}$, surface gravity $\log g$, metallicity [Fe/H]) and line-of-sight velocities V_l with random error of $5\ \mathrm{km\ s^{-1}}$ derived from the spectra using LSP3 (Xiang et al. 2015, 2017b) are available.

Precise parallaxes and proper motions of 1.3 billion stars in the Milky Way are now provided by the *Gaia* DR2 (Gaia Collaboration et al. 2018). Distances and asymmetric uncertainties are also available for those 1.3 billion stars in *Gaia* DR2 provided by Bailer-Jones et al. (2018), who derived the distances and uncertainties with a Bayesian method. In the current work, we adopt their distances. Line-of-sight velocities V_l for 7 million stars are also provided with an accuracy of $\sim 1\ \mathrm{km\ s^{-1}}$. Combining the distances, proper motions, and the line-of-sight velocities V_l of millions of stars provided by the *Gaia* DR2, we derive accurate 3D velocities of 7,224,631 (hereafter named the "*Gaia* sample") stars. 3D velocities of 3,600,275 (hereafter named the "*Gaia*-LAMOST sample") stars are also derived using the distances, proper motions from *Gaia* DR2 and V_l from the LAMOST surveys.

We estimate 3D velocities (U, V, W) and associated uncertainties of the individual stars using the method of Johnson et al. (1987). When we derive the errors of (U, V, W), the errors of distances, proper motions, and line-of-sight velocities are considered based on the the principle of uncertainty propagation. Then we transform (U, V, W) to (V_R, V_Φ, V_Z). Errors of (V_R, V_Φ, V_Z) are also estimated based on the principle of uncertainty propagation.

In order to obtain reliable results, we have removed stars with V_R, V_Φ, and V_Z uncertainties larger than $50\ \mathrm{km^{-1}}$, stars of distance uncertainties larger than 25%, and stars of $|V_R| > 400\ \mathrm{km\ s^{-1}}$, or $|V_\Phi - 240| > 400\ \mathrm{km\ s^{-1}}$, or $|V_Z| > 400\ \mathrm{km\ s^{-1}}$. Finally, the *Gaia* sample contains 6,150,394 stars, and the *Gaia*-LAMOST sample contains 3,344,860 stars.

3. Results

In this section, we examine the spatial variations of the phase spirals of V_Φ and V_R using the two samples. First, we divide the *Gaia* sample into six radial bins of R from 6.34 to 11.34 kpc and six azimuthal bins of Φ from $-6°$ to $6°$ to investigate the phase spirals of V_Φ and V_R in the different bins of R and Φ. Stars in the *Gaia*-LAMOST sample are also divided into six radial bins of R from 7.34 to 12.34 kpc to investigate the phase spirals of V_Φ and V_R at different R. The distribution of the *Gaia*-LAMOST sample stars in the Z–Φ plane is not symmetric, which is the consequence of the LAMOST sampling strategy, limiting magnitudes, and so on. Above the Galactic plane, most of the stars have negative values of Φ, whereas below the Galactic plane, most of the stars have positive Φ. Thus, we do not study the azimuthal variations of the phase spirals with the *Gaia*-LAMOST sample. When we explore the radial and azimuthal variations of the phase spirals, we adopt an azimuthal range Φ of $[-7.°5, 7.°5]$ and a radial range R of [7.84, 8.84] kpc, respectively. Likewise, when we examine the distributions of V_Φ and V_R in the Z–V_Z plane, we adopt bin sizes of $\Delta Z = 0.01$ kpc and $\Delta V_Z = 1.0\ \mathrm{km\ s^{-1}}$.

3.1. The Phase Spirals at Different Galactic Positions as Revealed by the Gaia Sample

3.1.1. Slicing by R

We first investigate the radial variations of the phase space spirals using the *Gaia* sample. Figure 1 shows the distributions of $V_\Phi - 228\ \mathrm{km\ s^{-1}}$ (left panels) and V_R (right panels) of the *Gaia* sample stars in the Z–V_Z plane and in the different radial bins. The radial range and number of stars in each bin are labeled in the figure.

The distributions of V_Φ show significant phase spirals. Our results confirm the previous finding of Antoja et al. (2018), Bland-Hawthorn et al. (2019), and Tian et al. (2018) for the Solar neighborhood. The phase spirals are apparent in all the

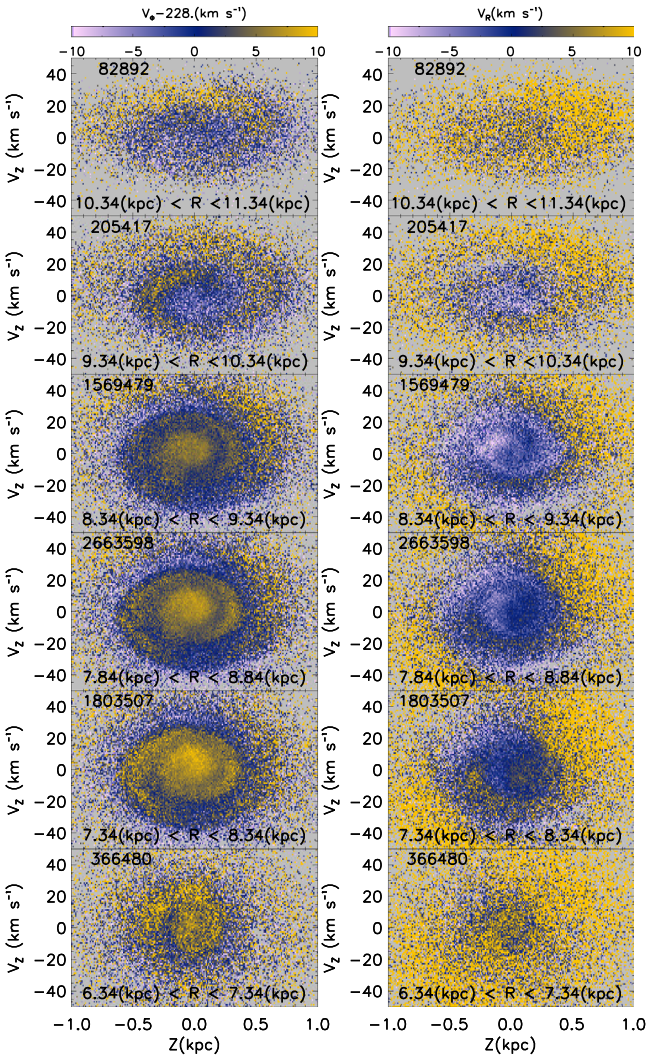

Figure 1. Distributions of median values of $V_\Phi - 228$ km s^{-1} (left panels) and V_R (right panels) of the *Gaia* sample stars in the Z–V_Z plane at different Galactic radii. The radial range and number of stars of each bin are labeled in each of the panels.

radial bins, especially in the bin of 6.34 kpc $< R <$ 10.34 kpc. The results strongly support the idea that the phase spirals are a disk-wide phenomenon (Bland-Hawthorn et al. 2019).

The phase spirals of V_Φ vary strongly with Galactic radius R as Figure 1 shows. The larger the R, the more relaxed the phase spirals. In Figure 1, the inner spirals become more and more relaxed as R increases, and essentially disappear at $R > 9.34$ kpc. The outer spirals are stronger in the outer disk than in the inner disk. One can find three spirals at $R < 9.34$ kpc, two spirals at $9.34 < R < 10.34$ kpc, and only one spiral at $10.34 < R < 11.34$ kpc in the phase space plane of $-1 < Z < 1$ kpc and $-50 < V_Z < 50$ km s^{-1}, which is consistent with the results of Laporte et al. (2019, see their Figure 14). The observed results presented here are consistent with the N-body simulation predictions of Bland-Hawthorn et al. (2019; see their Figure 22), who suggest that the stronger disk gravity in the inner disk leads to faster vertical oscillations and tighter phase spirals. In this scenario, one can see more spirals in the inner disk than in the outer disk in the same phase space region, which is indeed what one sees in Figure 1.

The distributions of V_R in the phase space plane at different Galactic radii are also presented in Figure 1. They show clear quadrupole patterns at all Galactic radii except that of $R > 10.34$ kpc; values of V_R are relatively small in the top-left and bottom-right parts of each right panels compared to those in the top-right and bottom-left corners. The quadrupole patterns, first mentioned by Bland-Hawthorn et al. (2019; see their Figure 16), are the consequence of the well-known tilt of the velocity ellipsoid (Siebert et al. 2008; Binney et al. 2014; Bland-Hawthorn et al. 2019). The quadrupole patterns are the clearest at 8.34 kpc $< R <$ 9.34 kpc, with the smallest V_R in the top-left and the bottom-right region, which is consistent with the previously observed radial velocity dip in the Solar neighborhood (Siebert et al. 2011; Huang et al. 2016; Carrillo et al. 2018; Tian et al. 2017).

At $7.34 < R < 10.34$ kpc, the phase spirals are also found in the distributions of V_R, which are broadly similar to those of V_Φ. However, the phase spirals are less tightly wound compared to those of V_Φ, which is again consistent with the numerical simulation results of Bland-Hawthorn et al. (2019). In the innermost ($R < 7.34$ kpc) and the outermost ($R > 10.34$ kpc) parts of the disk, the phase spirals are barely visible.

3.1.2. Slicing by Φ

We now investigate the distributions of V_Φ and V_R of the *Gaia* sample stars in phase space plane in different azimuthal bins. Figure 2 shows the main results. The azimuthal range and the number of stars in each bin are labeled in the figure.

The phase spirals of V_Φ are apparent in all azimuthal bins. Three spirals are clearly seen, with shapes that are quite similar. The phase spirals become stronger as Φ increases, are the strongest at $-2° < \Phi < 2°$, and then fade away as Φ further increases. Interestingly, the mean values of V_Φ at $-2° < \Phi < 2°$ are the smallest.

The distributions of V_R in the phase space plane in the different Φ bins are also presented in Figure 1. Similarly, the phase spirals are found in all the Φ bins, and are the strongest at $-2° < \Phi < 2°$. Quadrupole patterns are found in all the bins, and are also the strongest at $-2° < \Phi < 2°$.

3.2. The Phase Spirals at Different Galactic Positions as Revealed by the Gaia-*LAMOST* Sample

In order to verify the robustness of our detections of the phase spirals at different Galactic positions, we show in Figure 3 the V_Φ and V_R distributions of the *Gaia*-LAMOST sample in the Z–V_Z plane at different Galactic radii. What Figure 3 reveals is broadly similar to that seen in Figure 1.

Compared to Figure 1, the spiral patterns of V_Φ are less well resolved by the *Gaia*-LAMOST sample stars, especially for the inner spirals in the inner disk ($7.34 < R < 9.34$ kpc). As mentioned in Section 2, line-of-sight velocities of the *Gaia*-LAMOST sample stars are much less accurate than those of the *Gaia* sample. This is responsible for the aforementioned difference. In Figure 3, the phase spirals in outer disk ($R > 9.34$ kpc) are much stronger than those seen in Figure 1. This may be partly due to the fact that stars in the *Gaia*-LAMOST sample have smaller mean values of the absolute azimuthal angle compared to those of the *Gaia* sample stars at $R > 9.34$ kpc, which is consistent with the results of Section 3.1.2.

In Figure 3, the distributions of V_R in the phase space plane are broadly consistent with that seen in Figure 1, but less

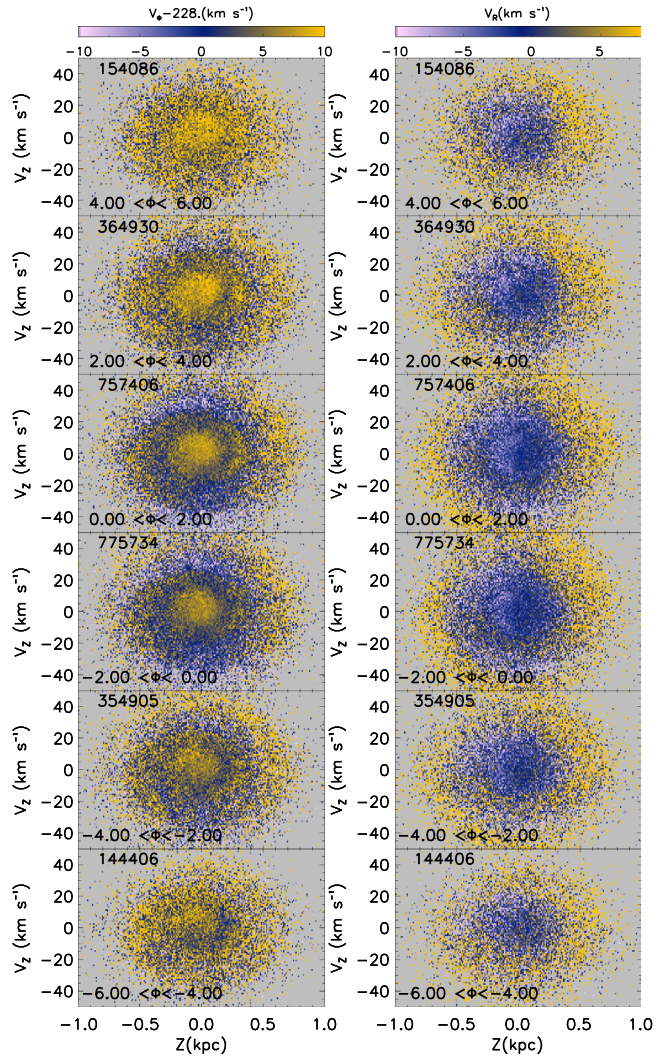

Figure 2. Distributions of median values of $V_\Phi - 228$ km s^{-1} (left panels) and V_R (right panels) of the *Gaia* sample stars in the Z–V_Z plane at different azimuthal angles. The azimuthal angle range and the number of stars are labeled in each of the panels.

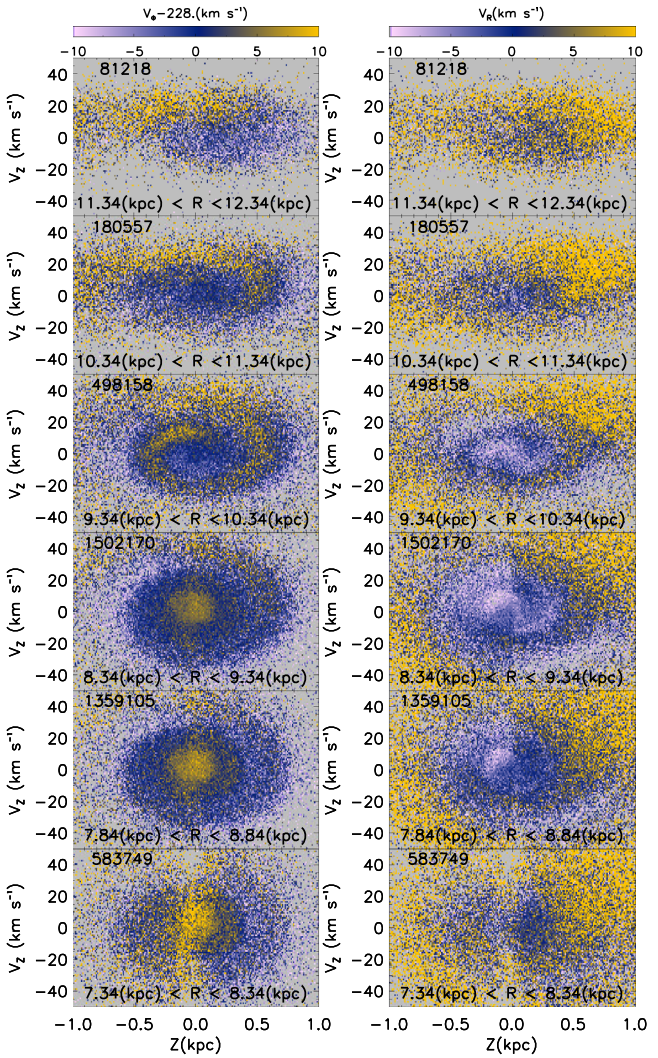

Figure 3. Similar to Figure 1 but for the *Gaia*-LAMOST sample. The radial range is from 7.34 to 12.34 kpc.

clearly. The quadrupole patterns are also similar to those uncovered by the *Gaia* sample. In Figure 3, the quadrupole patterns are seen even at $R > 10.34$ kpc. This is not the case when using the *Gaia* sample. The reason is that stars in the *Gaia*-LAMOST sample have smaller mean values of $|\Phi|$ than those of the *Gaia* sample, considering that the spiral and quadrupole patterns of stars of smaller $|\Phi|$ are stronger than those of larger $|\Phi|$. Moreover, there is a clear break of V_R from south side ($Z < 0$ kpc) to north ($Z > 0$ kpc), especially in the range of $7.84 < R < 9.84$ kpc. We suggest that it might be caused by the quadrupole patterns of the spirals, the bright limiting magnitudes, and very low sampling rates of the LAMOST surveys in the solar neighborhood after a careful check.

4. Discussion

4.1. The Effects of 3D Velocity Errors on the Phase Spirals

As discussed in Section 3.1.1, there are three phase spirals of V_Φ in the inner disk ($R < 9.34$ kpc), but only one or two phase spirals in the outer disk ($R > 9.34$ kpc). Meanwhile, the errors of the 3D velocities of stars at $R > 9.34$ kpc are larger than those of stars at $R < 9.34$ kpc. In order to check the relationship between spiral numbers and velocity errors, we use the Monte Carlo method to check if the spirals in the range of [7.84, 8.84] kpc are still robust. We first increase the errors of 3D velocities of each star at $7.84 < R < 8.84$ kpc by scaling with a factor, which is estimated as the ratio of the mean random velocity errors of stars at $9.34 < R < 10.34$ kpc and those of stars at $7.84 < R < 8.84$ kpc. The final velocities of the stars are derived by adding the errors, which are randomly generated assuming Gaussian distributions, with the increased errors as the dispersions. We then examine the resultant V_Φ and V_R distributions in the phase plane. The process is repeated 1000 times, and the resultant 1000 distributions of V_Φ and V_R are quite similar one to the other.

Figure 4 shows one of the resultant V_Φ and V_R distributions in the phase space plane before and after increasing the velocity errors for stars at $7.84 < R < 8.84$ kpc. The phase spirals of V_Φ and V_R seen show negligible differences before and after increasing the velocity errors. We therefore conclude that the results of more relaxed phase spirals of V_Φ in the outer disk are authentic.

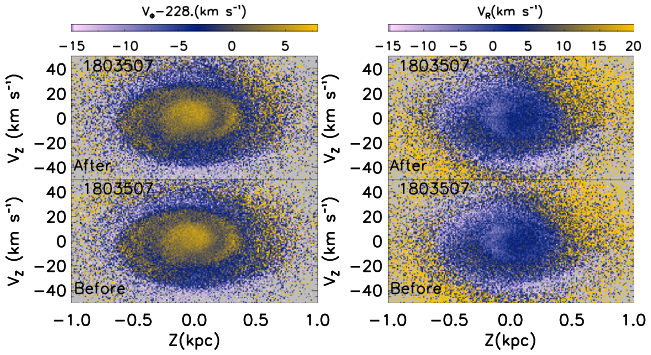

Figure 4. Distributions of $V_\Phi - 228$ km s^{-1} (left panels) and V_R (right panels) in the Z–V_Z plane for stars at $7.84 < R < 8.84$ kpc, before (bottom panels) and after (top panels) increasing the velocity errors.

4.2. Origins of Phase Spirals

Our results as revealed by both the *Gaia* and the *Gaia*-LAMOST samples suggest that the phase space spirals of V_Φ become more relaxed as R increases. The phenomenon is exactly predicted by the N-body simulations of Bland-Hawthorn et al. (2019) and Laporte et al. (2019), who suggested that the passage of the Sagittarius through the Galactic plane, a scenario of an external origin, produces the vertical phase-mixing and phase spirals. The predicted radial variations of the phase spirals of V_Φ as driven by buckling of the stellar bar (internal origin; Khoperskov et al. 2018) are on the other hand not so consistent with the conclusion of Laporte et al. (2019). Our results suggest instead an origin of the phase spirals that are developed from an external perturbation.

If this scenario of an external origin is true, the location of the intruder passing through the Galactic plane and the mass and passage duration of the intruder become important issues. An intruder will attract stars to it, changing their 3D velocities as the intruder passes through the Galaxy (Binney & Schönrich 2018, see their Figures 1 and 2). Meanwhile, the phase spirals at different Galactic positions, especially its radial and azimuthal variations, are no doubt strongly affected by the aforementioned parameters of the intruder. In other words, one can study the intruding passage location and duration through the radial and azimuthal variations of the phase spirals of V_Φ and V_R.

When an intruder passes through the Galactic plane, the effect of the intruder on the star in the line of the Galactic center and the intruder is largest, and the phase spiral in this direction is clearest. In Figure 2, we find that the phase spirals of V_Φ and V_R are clearest at $-2° < \Phi < 2°$, and become weaker as $|\Phi| > 2°$. It suggests that the external intruder passes through the Galactic plane in the direction of the Galactic center or anti-center.

The phase spirals of V_Φ and V_R at $4° < \Phi < 6°$ and $-6° < \Phi < -4°$ are significantly weaker, almost invisible, suggesting that the speed of the intruder is quite fast such that it mainly affects stars within an azimuthal angle range of 8°, or about 2% of the rotation period of a star at a Galactic radius $R \approx R_0$. The volume that the intruder can affect is also directly linked to its mass; a more massive intruder can affect a larger volume.

As discussed in the previous works, the most probably perturbation source is the Sagittarius dwarf, which has a "trefoil" orbit over the past 2.3 Gyr. It crossed the disk about 420 Myr ago at $R = 13$ kpc and transited again about 50 Myr ago (Law et al. 2005; Bland-Hawthorn et al. 2019; Tepper-García & Bland-Hawthorn 2019). If the Sagittarius dwarf is responsible for the phase spirals, the results presented here can help constrain its orbit and mass, even the shape of the Galactic halo. Detailed modeling is required to reproduce the observed spatial variations of the phase spirals of V_Φ and V_R.

5. Summary

In this Letter, we study the phase space spirals of V_Φ and V_R using the *Gaia* and LAMOST data, and investigate the radial and azimuthal variations of the spiral and quadrupole patterns in the phase space plane. The main results are as follows.

1. The distributions of V_Φ in the Z–V_Z plane show strong spiral patterns at $6.34 < R < 12.34$ kpc.
2. The phase spirals of V_Φ become more relaxed as R increases.
3. The distributions of V_R in the Z–V_Z plane show strong quadrupole patterns in all R and Φ bins. They also show spiral patterns but not so tightly wound as those of V_Φ. In the innermost ($R < 7.34$ kpc) and outermost disk ($R > 10.34$ kpc), the spiral patterns are barely visible.
4. The spiral patterns of V_Φ and the quadrupole and spiral patterns of V_R in the Z–V_Z plane are the strongest at $-2° < \Phi < 2°$, but almost invisible at $4° < \Phi < 6°$ and $-6° < \Phi < -4°$.

The radial variations of the phase spirals of V_Φ are consistent with the predictions of perturbation by an external intruder as suggested by Bland-Hawthorn et al. (2019) and Laporte et al. (2019), but are inconsistent with an internal origin as suggested by Khoperskov et al. (2018). The azimuthal variations of the phase spirals of V_Φ and V_R suggest that the intruder passes through the Galactic plane in the direction of either the Galactic center or the anti-center. The azimuthal variations of the phase spirals of V_Φ and V_R also tell us something about the mass and the passage duration of the intruder. A detailed model is required to reproduce the results presented here.

This work is supported by the National Natural Science Foundation of China 11833006, U1531244, 11811530289, U1731108, 11803029, and 11473001 and the Yunnan University grant No. C176220100006. Guoshoujing Telescope (LAMOST) is a National Major Scientific Project built by the Chinese Academy of Sciences. Funding for the project has been provided by the National Development and Reform Commission. LAMOST is operated and managed by the National Astronomical Observatories, Chinese Academy of Sciences. The LAMOST FELLOWSHIP is supported by Special Funding for Advanced Users, budgeted and administrated by Center for Astronomical Mega-Science, Chinese Academy of Sciences (CAMS).

References

Antoja, T., Helmi, A., Romero-Gómez, M., et al. 2018, Natur, 561, 360
Bailer-Jones, C. A. L., Rybizki, J., Fouesneau, M., Mantelet, G., & Andrae, R. 2018, AJ, 156, 58
Binney, J., Burnett, B., Kordopatis, G., et al. 2014, MNRAS, 439, 1231
Binney, J., & Schönrich, R. 2018, MNRAS, 481, 1501
Bland-Hawthorn, J., Sharma, S., Tepper-Garcia, T., et al. 2019, MNRAS, 486, 1167
Bovy, J., Bird, J. C., García Pérez, A. E., et al. 2015, ApJ, 800, 83
Carlin, J. L., DeLaunay, J., Newberg, H. J., et al. 2013, ApJL, 777, L5
Carrillo, I., Minchev, I., Kordopatis, G., et al. 2018, MNRAS, 475, 2679

Deng, L.-C., Newberg, H. J., Liu, C., et al. 2012, RAA, 12, 735
Gaia Collaboration, Brown, A. G. A., Vallenari, A., et al. 2018, A&A, 616, A1
Gómez, F. A., Minchev, I., O'Shea, B. W., et al. 2013, MNRAS, 429, 159
Huang, Y., Liu, X.-W., Yuan, H.-B., et al. 2015, MNRAS, 449, 162
Huang, Y., Liu, X.-W., Yuan, H.-B., et al. 2016, MNRAS, 463, 2623
Johnson, D. L., Koplik, J., & Dashen, R. 1987, JFM, 176, 379
Khoperskov, S., Di Matteo, P., Gerhard, O., et al. 2019, A&A, 622, L6
Laporte, C. F. P., Minchev, I., Johnston, K. V., & Gómez, F. A. 2019, MNRAS, 485, 3134
Law, D. R., Johnston, K. V., & Majewski, S. R. 2005, ApJ, 619, 807
Liu, X.-W., Yuan, H.-B., Huo, Z.-Y., et al. 2014, in IAU Symp. 298, Setting the Scene for Gaia and LAMOST, ed. S. Feltzing (Cambridge: Cambridge Univ. Press), 310
Reid, M. J., Menten, K. M., Brunthaler, A., et al. 2014, ApJ, 783, 130
Schönrich, R., Binney, J., & Dehnen, W. 2010, MNRAS, 403, 1829
Siebert, A., Bienaymé, O., Binney, J., et al. 2008, MNRAS, 391, 793
Siebert, A., Famaey, B., Binney, J., et al. 2012, MNRAS, 425, 2335
Siebert, A., Famaey, B., Minchev, I., et al. 2011, MNRAS, 412, 2026
Sun, N.-C., Liu, X.-W., Huang, Y., et al. 2015, RAA, 15, 1342
Tepper-García, T., & Bland-Hawthorn, J. 2019, MNRAS, 478, 5263
Tian, H.-J., Liu, C., Wan, J.-C., et al. 2017, RAA, 17, 114
Tian, H.-J., Liu, C., Wu, Y., Xiang, M.-S., & Zhang, Y. 2018, ApJL, 865, L19
Wang, H., López-Corredoira, M., Carlin, J. L., & Deng, L. 2018, MNRAS, 477, 2858
Williams, M. E. K., Steinmetz, M., Binney, J., et al. 2013, MNRAS, 436, 101
Xiang, M., Liu, X., Shi, J., et al. 2017a, ApJS, 232, 2
Xiang, M.-S., Liu, X.-W., Shi, J.-R., et al. 2017b, MNRAS, 464, 3657
Xiang, M. S., Liu, X. W., Yuan, H. B., et al. 2015, MNRAS, 448, 822
Yuan, H.-B., Liu, X.-W., Huo, Z.-Y., et al. 2015, MNRAS, 448, 855
Zhao, G., Zhao, Y.-H., Chu, Y.-Q., Jing, Y.-P., & Deng, L.-C. 2012, RAA, 12, 723